April 2004

Imaging and Characterization of Molecules and One-Dimensional Crystals Formed within Carbon Nanotubes

Jeremy Sloan

David E. Luzzi
University of Pennsylvania, luzzi@lrsm.upenn.edu

Angus I. Kirkland

John L. Hutchison

Malcolm L.H. Green

Imaging and Characterization of Molecules and One-Dimensional Crystals Formed within Carbon Nanotubes

Abstract

The imaging and characterization of individual molecules and atomically thin, effectively one-dimensional crystals of rock salt and other halides encapsulated within single-walled carbon nanotubes are reviewed in this article. These species were imaged by conventional and super-resolved high-resolution transmission electron microscopy and by scanning tunneling microscopy, revealing the detailed atomic structure of these nanoscopic species.

Keywords

carbon nanotubes, crystal growth, fullerenes, nanocomposites, scanning tunneling microscopy, transmission electron microscopy

Imaging and Characterization of Molecules and One-Dimensional Crystals Formed within Carbon Nanotubes

J. Sloan, D.E. Luzzi, A.I. Kirkland, J.L. Hutchison, and M.L.H. Green

Abstract

The imaging and characterization of individual molecules and atomically thin, effectively one-dimensional crystals of rock salt and other halides encapsulated within single-walled carbon nanotubes are reviewed in this article. These species were imaged by conventional and super-resolved high-resolution transmission electron microscopy and by scanning tunneling microscopy, revealing the detailed atomic structure of these nanoscopic species.

Keywords: *carbon nanotubes, crystal growth, fullerenes, nanocomposites, scanning tunneling microscopy, transmission electron microscopy.*

Introduction

The synthesis, characterization, and modification of individual molecules, one-dimensional (1D) crystals, and other species formed within single-walled carbon nanotubes (SWNTs) have been investigated in several laboratories. These species have been imaged using techniques such as conventional and super-resolved high-resolution transmission electron microscopy (HRTEM) and scanning tunneling microscopy (STM). In appropriately dispersed specimens, it has been possible to image the encapsulated species in several ways: as discrete molecules; 1D arrays, helical chains, and clusters of molecules; disordered or glassy fillings; randomly oriented clusters; and continuously aligned or helically distorted 1D crystals. In the case of 1D crystals, these are constrained in cross section by the van der Waals surface of the encapsulating SWNTs, forming so-called Feynman crystals—effectively, integral numbers of atomic layers in terms of their thickness, specified by the diameter of the encapsulating tube.[1] The ability of carbon nanotubes—in particular, SWNTs—to "fix" individual molecules or discrete crystals 2–3 atomic layers thick for direct imaging is fostered by their extremely small internal diameters, which exist within a very restricted range of ~0.4–5 nm with a median of only 1–2 nm. When the van der Waals surfaces of the wall carbons are taken into account, the effective internal diameters (IDs) of the SWNTs are reduced by ~0.35 nm, thus producing cylinders with effective IDs of 0.7–1.7 nm.

These nanocomposites represent a new generation of materials that can be synthesized on a bulk scale and potentially form the basis of diodes,[2–4] single-electron transistors,[5,6] memory elements,[7] and logic circuits.[8] For example, Yao and co-workers[2] showed in 1999 how it was possible to make an intramolecular junction between two SWNTs, one semiconducting and one metallic, thus forming the basis of a rectifying diode. Recently, substantial progress has been made with respect to the comprehensive characterization of the filled nanocomposites. Of particular importance in this regard are

1. The component crystal structures of the encapsulating nanotubes, which may be conveniently reduced to the (n,m) chiral indices defining the sp^2 carbon cylinder according to the equation

$$\mathbf{C}_h = n\mathbf{a}_1 + m\mathbf{a}_2, \quad (1)$$

where $\mathbf{C}_h$ is the roll-up vector, which defines the different ways in which a 2D graphene sheet can roll up to form a nanotube, and $\mathbf{a}_1$ and $\mathbf{a}_2$ are the basal vectors of the parent 2D carbon lattice;
2. The conformation, packing behavior, or crystal structure of the encapsulated molecules or 1D crystals.

Only when both of these components can be interpreted quantitatively—in terms of individual filled tubes or, more ideally, the bulk composite sample—can their physical properties be fully understood in a theoretical or experimental sense and therefore be further developed in terms of practical applications. This article highlights some of the more significant developments that have been made with regard to the complete characterization of filled-nanotube nanocomposites.

SWNT Encapsulation Methodologies

Insertion of Crystalline and Noncrystalline Materials into SWNTs

The first crystalline materials inserted within SWNTs were clusters and 1D nanowires of Ru metal formed by immersing a sample of acid-treated SWNTs in a saturated solution of $RuCl_3$.[9] Following H_2 reduction, a filling of approximately of 2–5% of all the observed SWNTs with Ru metal was observed. Acidification was considered necessary in order to open the tips of the SWNTs, which were assumed to be closed. Subsequently, SWNTs were filled without acidification by capillary wetting with molten mixtures of silver halides or mixtures of alkali halides and actinide halides.[10] The ability of a molten material to wet and fill SWNTs depends on the

wetting criterion determined by Ebbesen for the filling of nanotubes with liquid-phase media.[11] In general, the filling procedure entails heating as-made nanotubes with the molten salt or oxide to a temperature 100 K above the respective melting point of the filling material. Improvements in filling yield (from 20–30% to more than 50–70%) can be achieved by thermally cycling the filling material from the filling temperature to 100 K below this temperature.[12] The excess filling material may be removed without removing the encapsulated material by gently washing the filled composite with cool or warm water or dilute HCl. Mixtures of predominantly amorphous ternary-phase materials may similarly be introduced into SWNTs by exploiting the melting properties of the relevant phases.[10] SWNTs can now be filled with a wide range of solid-phase crystalline and noncrystalline materials including metals and metal salts,[1,9,10] oxides,[13,14] and helical iodine chains.[15]

Further modifications are possible on such materials once they are incorporated within SWNTs. For example, for SWNTs filled with silver halides, the halide undergoes spontaneous photolytic decomposition, resulting in the formation of aligned 1D fcc silver nanowires.[10] Similarly, it has been possible to reduce incorporated $RuCl_3$ to the base metal (see preceding paragraph), and the formation of reduced lanthanide nanowires has also been reported.[16] As with encapsulated fullerene or endofullerene molecules, *in situ* e^- beam reduction in a high-resolution transmission electron microscope can modify the filling material to form reduced clusters, as in the case of $ZrCl_4$ formed within SWNTs.[17]

Insertion of Molecules into SWNTs

In addition to the incorporation of crystalline and noncrystalline materials into SWNTs, it has also been possible to insert and directly image molecular structures within the internal cavities of the nanotubes. The first such imaged species were C_{60} molecules formed within nanotubes produced by laser ablation, resulting in SWNT composite structures called peapods (see Figures 1a and 1b).[18] Quantitative filling of SWNTs with fullerenes[19,20] or endofullerenes[21] has since been effected by gas-phase diffusion of heat-treated SWNT samples. In these experiments, the SWNTs were annealed in vacuum up to 450°C or in dry air up to 420°C, resulting in continuous filling of all the observed SWNTs with fullerenes. These treatments help dissipate moisture and eliminate other capillary-absorbed species from within the tubes and therefore improve the filling yield.

More recently, non-fullerene molecular species have been inserted into SWNTs. These include metallocenes, molecular halides, and *ortho*-carborane molecules.[22,23] Metallocenes—for example, ferrocene—and molecular halides may be introduced into SWNTs by the capillary wetting method described in the previous section. *Ortho*-carborane was introduced into SWNTs by gentle sublimation at temperatures of 350–420°C. SWNTs can also be filled by a variety of organic molecules, including tetrathiafulvalene (TTF), tetramethyl-tetraselenafulvalene (TMSF), and tetracyano-*p*-quinodimethane (TCNQ).[24] Optical-absorption spectroscopy revealed that SWNTs doped with TTF and TMSF behaved like *n*-type semiconductors, while those doped with TCNQ behaved like *p*-type semiconductors.

Characterization of SWNT Encapsulates

Spectroscopy and Bulk Techniques Applied to Filled SWNT Samples

As will be shown in a later section, it is possible to use HRTEM and other microscopies to characterize individual filled SWNTs. To some extent, the same techniques can be used statistically to screen bulk filled samples in order to assess the filling yield or to study changes in the encapsulated materials. In at least one respect, however, such imaging methods can never be truly quantitative, as it is impossible in practical terms to screen an entire specimen using local imaging techniques that, at best, are capable of a field of view of fractions of a micrometer. This means that important specimen features, such as sample inhomogeneities or impurities, may inadvertently be missed during the specimen screening process. Additionally, it is often difficult to follow subtle changes in a bulk sample as it undergoes time- or temperature-dependent modification. There is therefore a need to supplement such local probe screening methods with bulk analytical tools; there has been considerable recent progress in this regard.

Bulk SWNT samples self-organize into ordered crystalline ropes upon annealing. The arrays formed within the nanotube

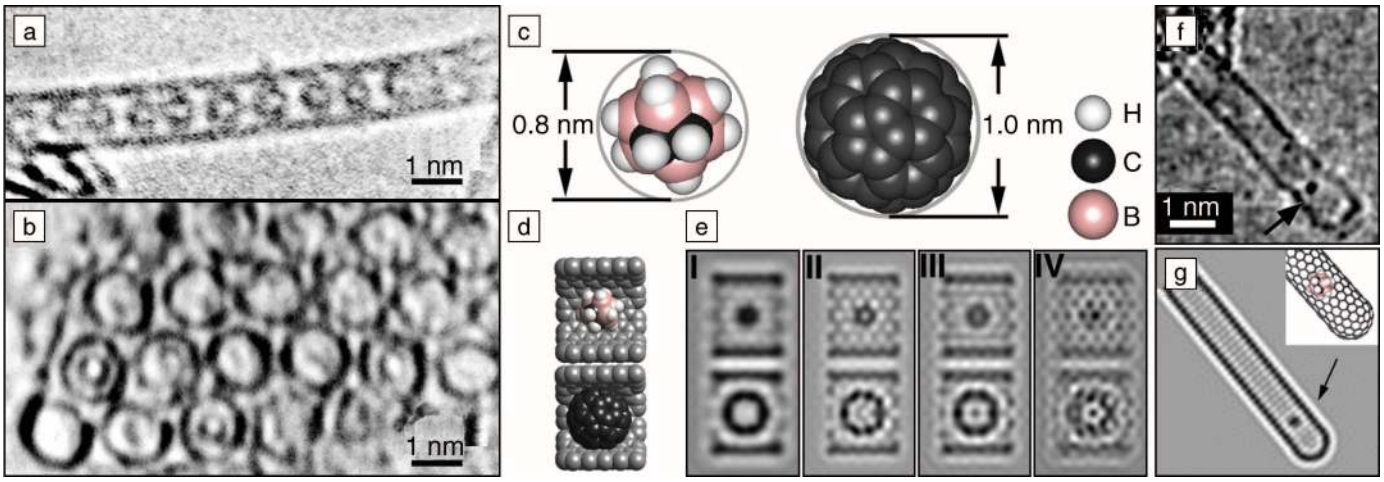

Figure 1. (a) High-resolution transmission electron microscopy (HRTEM) image obtained at 100 kV, showing the first example of a single-walled nanotube (SWNT) filled with C_{60} molecules. (b) Second image from the same specimen as in (a), showing a cross-sectional view of an ordered bundle of SWNTs, some of which are filled with fullerenes. (c) Structure models indicating the outside diameters of ortho*-carborane (left) and C_{60} (right). (d), (e) Packing models and corresponding focal series images showing the different imaging properties of* ortho*-carborane (top set of images) and C_{60} (bottom set of images) inside fragments of (10,10) SWNTs. (f), (g) HRTEM image and corresponding image simulation (with model inset), showing a single* ortho*-carborane molecule formed within the tip of a SWNT. (From References 18 and 23.)*

ropes give rise to prominent scattering, due to the obtained 2D triangular lattice observable by bulk x-ray diffraction (XRD).[25] Synchrotron x-ray scattering experiments performed on fullerene-filled SWNTs have recently shown that ovoid or "rugby ball"-shaped C_{70} molecules align along the capillaries according to two arrangements: "standing," in which the ovoid molecules align perpendicular to the tube axis; and "lying," in which they align parallel to the SWNT axes.[26] These two conformations were determined from additional lattice spacings observed in the synchrotron powder patterns that were attributed to the 1D lattice spacings of the molecules as they lined up along the SWNTs. Moreover, the same researchers reported pronounced differential thermal distortions for the two conformations with the diffraction peaks, due to the standing conformation showing a much greater temperature dependence and propensity to lattice expansion than the lying conformation. Quantitative XRD experiments have also been used to establish the filling factor of nanotube composites and may also be used to assess the degree of graphitic or other impurities present in SWNT samples. The filling factor may be established by comparing the experimental and computed structure factors of fullerene-filled and unfilled crystalline SWNT samples, respectively.[26,27]

Another technique that has recently been used to characterize bulk filled SWNT samples is optical spectroscopy.[27] Both laser Raman and optical absorption spectroscopy have been used to characterize SWNTs filled with fullerenes and nonfullerenes (i.e., zinc diphenylporphyrin, Zn-DPP). Time-resolved Raman studies revealed a reduction in the characteristic vibrational mode [i.e., Ag(2)], that distinguishes the C_{60} molecules from their host nanotubes, when SWNT composites filled with the fullerenes were irradiated with blue laser light ($\lambda = 488$ nm). Corresponding broadening of additional fullerenic vibrational modes [i.e., Hg(1)] in temperature-resolved experiments further indicated the formation of dimers, trimers, or oligomers, suggesting that photopolymerization of the fullerenes had occurred within the SWNTs. Elsewhere (see the article by Bandow et al. in this issue), the use of Raman spectroscopy to monitor the formation of DWNTs from fullerene-filled SWNTs has been reported. In general, the encapsulation of fullerenes within SWNTs leads to a shifting of the characteristic breathing modes (i.e., vibrational modes associated with the expansion and contraction of the SWNTs, hence the term "breathing") to a lower wavelength, although when the C_{60}-filled samples are annealed to 1473 K, new radial breathing modes corresponding to the paired inner SWNTs formed by polymerization of the encapsulated fullerenes are observed. SWNTs filled with Zn-DPP similarly show a downshifting of the characteristic Raman breathing modes relative to unfilled tubes.[27]

Electron Diffraction

As described in the previous section, the self-organization of fullerene molecules along SWNT capillaries leads to the formation of 1D crystals. Electron diffraction and direct imaging techniques can be utilized to extract information from individual SWNTs, often with a precision approaching that of XRD techniques. Recent work has shown that semiquantitative analysis of selected-area electron diffraction (SAED) patterns obtained from empty DWNTs permit retrieval of the chiral indices of the component tubules for nanotubes with diameters of up to 4 nm.[28] This approach is essentially an extension of similar diffraction experiments originally implemented to establish the chiral nature of multiwalled nanotubes[29] and consists of extracting diffraction intensities from patterns obtained using a high-coherence field-emission gun electron source. Simulation of the diffracted intensity for all possible component (n,m) SWNTs and extensive comparison of these intensities with kinematic theory suggested that the component chiral indices of the two constituent nanotubes could be retrieved with reasonable precision.[28] Similar results were reported for localized regions of SWNTs using nanobeam electron diffraction.[30] In perhaps an even more remarkable experiment, Zuo et al. have shown that it is possible to extract the phase information from DWNT SAED, with the result that the 2D crystal structure of the parent nanotube can be reconstructed in an experimental and theoretical approach analogous to the solution of the phase problem in x-ray crystallography.[31] In parallel developments,[32] Kramberger and co-workers have also shown how (n,m) chiral indices can also be assigned to inner and outer SWNTs in DWNTs from experimentally obtained Raman radial breathing modes.

With respect to the interpretation of SWNT-incorporated species, direct electron diffraction measurements have predominantly been confined to determining the lattice spacings within 1D crystals of incorporated fullerene molecules within peapod encapsulates. SAED pattern measurements from bundles of SWNTs filled with fullerenes of different sizes and shapes have so far shown that the intermolecule separations are in fact 3–4% smaller than those measured for the corresponding bulk fullerene crystals,[33] in which the molecules are separated by slightly less than the van der Waals graphene separation (~0.34 nm).

Imaging of Encapsulated Species by Conventional and Super-Resolved HRTEM

Direct lattice imaging by conventional HRTEM can be used to image molecular species and aligned 1D crystals formed within SWNTs. Indeed, the technique has proved invaluable, since both the microstructure and the helical nature of multilayer nanotubes were correctly demonstrated by a combination of HRTEM and electron diffraction in 1993.[29] More recently, considerable progress has been made with regard to the imaging of SWNT-incorporated molecules and 1D crystals by direct, super-resolved, and spectroscopic methods.

With respect to the imaging of species formed within SWNTs by HRTEM, five considerations are paramount in obtaining the maximum level of information: (1) the spatial resolution of the imaging technique being used, (2) the imaging properties of the encapsulated specimen, (3) the structural chemistry of the incorporated specimen and the encapsulating nanotube, (4) the relative stability of the encapsulated specimen with respect to the imaging technique and conditions being used, and (5) the degree of 3D information that may be obtained from the respective technique. As will be seen in the case of 1D CoI_2 incorporated within a SWNT, it is possible to extrapolate (5) from certain kinds of information available in 2D projections of directly imaged specimens, but further advances in instrument design are still needed, particularly HRTEM specimen holders, before true 3D information of these nanocomposites will be available at the atomic level.

The spatial resolution of HRTEM is principally governed by the quality of the main imaging objective lens, which may be expressed in terms of the spherical aberration coefficient C_s. The consequence for conventional HRTEM is that the point resolution is reduced to 0.16–0.3 nm for most commercial instruments. For most materials imaged with HRTEM, it is therefore possible to resolve individual strongly scattering atoms and ordered columns or clusters of more weakly scattering atoms imaged in projection. Thus, for the example in Figure 2a, we see a conventional HRTEM image obtained at close-to-optimum Scherzer defocus conditions of a 2×2 potassium iodide (KI) crystal formed within a SWNT ~1.4 nm in diameter.[34] In this image, the I–K or K–I columns are clearly resolved (see the structure model

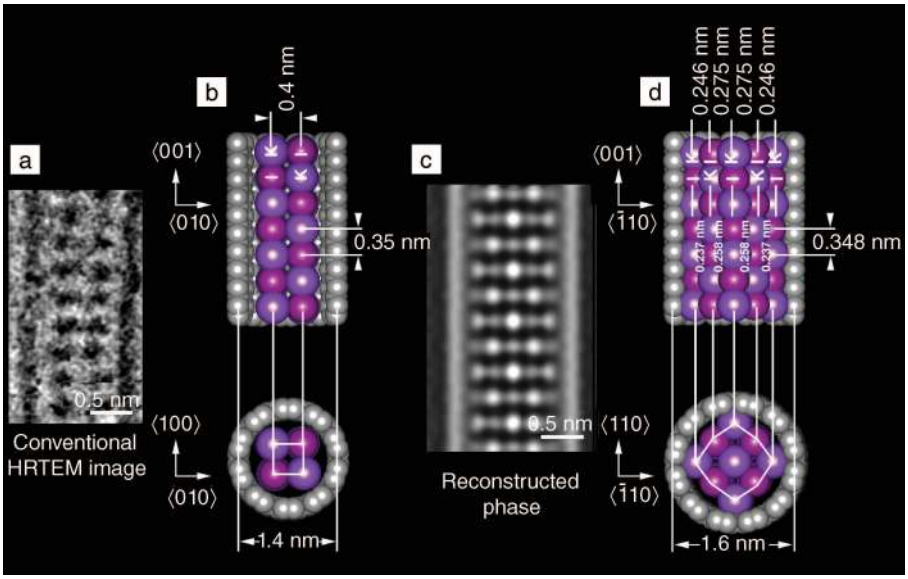

Figure 2. (a) Conventional high-resolution transmission electron microscopy (HRTEM) image of a 2 × 2 KI crystal formed within a ~1.4-nm-diameter single-walled carbon nanotube (SWNT). (b) Structure model derived from (a). (c) Super-resolved HRTEM image of a 3 × 3 KI crystal formed in a ~1.6-nm-diameter SWNT. (d) Corresponding structure model derived from (c). (From References 29 and 34.)

in Figure 2b), whereas the graphene walls appear as continuous and featureless parallel black lines. Similarly, in the images and simulations of fullerenes and carborane molecules shown in Figure 1, the nanotubes appear as parallel black lines, and the encapsulated molecules appear either as black circles, in the case of the fullerenes (cf. Figures 1a, 1b, and top images in 1e) or as indistinct blurred spots, as in the case of the carboranes (cf. bottom images in Figure 1e; Figures 1f and 1g). In these cases, the contrast is due to columns of superposed carbon or boron and carbon atoms. Under such imaging conditions, however, information from discrete atom columns of light elements is unavailable. In the example in Figure 2a, only the strongly scattering I atoms ($Z = 53$) contribute significantly to the image contrast, while the K atoms ($Z = 19$) make a negligible contribution.

Considerable enhancement of the detail available from conventional HRTEM images is possible, provided that the sample is stable enough [see (4) mentioned earlier in this section]. This can be achieved by restoring the exit plane wave of the electron beam propagating from the specimen from either a tilt or focal series of HRTEM images.[35–37] In doing so, several key aberrations

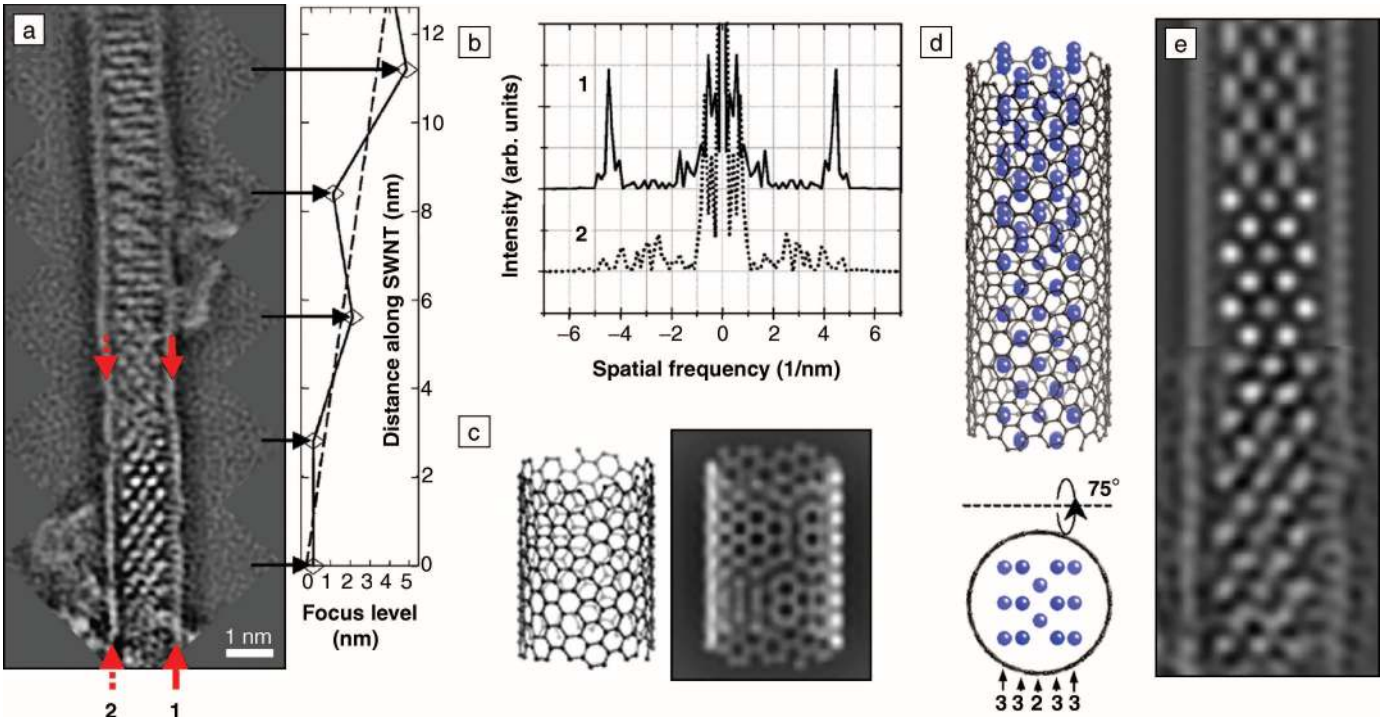

*Figure 3. (a) Super-resolved high-resolution transmission electron micrograph recorded from a Sb_2O_3/single-walled carbon nanotube (SWNT) nanocomposite. To the right of the image is a plot of focus level versus distance along the SWNT. (b) One-dimensional power spectra (fast Fourier transform) obtained from the two opposing walls [e.g., **1** and **2** in (a)] of the SWNT. (c) Derived conformation and simulation of the encapsulating SWNT in (a). (d) Structure model of encapsulate (Sb atoms indicated in blue). (e) Comparison of multislice simulation produced from (d) (top image) and experimental image (bottom image). (From Reference 14.)*

may be removed, with the result that information can be obtained out to or beyond the information limit rather than the point resolution (e.g., 0.1 nm as opposed to 0.16 nm for a JEOL 300 kV field-emission gun TEM). Further improvements in instrument technology and image processing are under way at Oxford and in other laboratories, which should improve this resolution limit still further. For example, the direct imaging of Li atom columns was recently reported for macroscopic crystals of $LiCoO_2$ imaged in by HRTEM at ~0.8 nm resolution by Shao-Horn and co-workers.[38]

In Figure 2c, we see an example of a super-resolved image of 3 × 3 KI formed within a ~1.6-nm-diameter SWNT and, in Figure 2d, the corresponding derived structure model.[39] As the encapsulated crystal is visible in a [110] projection relative to bulk KI, all of the atom columns are visible as pure atom columns. In the conventional image (not shown), the heavy I atoms are visible, whereas the K atoms are invisible. In the case of the reverse-contrast restored image (Figure 2c), we see that the I columns are much more prominent, but are now interspersed with the weaker K columns. A further key point is that the intensities of the bright spots corresponding to the I and K columns are modulated according to atom column thickness. Thus, along the SWNT, we can easily identify two alternating layers corresponding to I-2K-3I-2K-I and K-2I-3K-2I-K, consistent with the 3 × 3 × ∞ 1D KI crystal. It is worth noting that both 1D crystals display considerable lattice distortions as compared with their bulk structures. In the 2 × 2 case, a lattice expansion of ~17% occurs across the SWNT capillary, whereas in the 3 × 3 case, a differential expansion is observed, with the I columns being more compressed than the K columns (see Figure 2d).

Another advantage of the focal series technique is that by restoring subregions of a composite image, the height of each subregion relative to each contiguous subregion can be computed, and this gives a measure of the tilt angle of the SWNT as viewed in the HRTEM.[14] This information can be confined with imaging information obtained from the SWNT walls, which under favorable conditions will provide information about the conformation of the encapsulating SWNT. In Figure 3a, we can see a reconstructed phase image of a 1D crystal of Sb_2O_3 formed within a ~1.45-nm-diameter SWNT. By examining the image and the absolute focus level along the length of the SWNT (see plot in Figure 3a), we can easily establish that this is a tilted SWNT and that the angle of tilt with respect to the plane of the image is ~15°. In addition to this information, we can also see that at the bottom of the image, the encapsulated 1D crystal is resolved as a 2D array of atom columns, and that along indicated direction **1**, that wall carbons, with a spacing of 0.224 nm, are clearly visible. No such contrast is evident on the left-hand wall, indicated by **2**. The spatial frequencies along the nanotube walls were extracted accurately from 1D power spectra (or fast Fourier transform, Figure 3b), and these were exhaustively compared against spatial frequencies computed for all SWNTs with diameters in a similar range to the experimental case. A candidate tube with a conformation of (21,–8) [being the mirror image of (13,8)] was chosen in order to simulate the experimental case (Figure 3c). It is significant that a detailed analysis of both the carbon wall contrast and the nanotube tilt gives us unambiguously the "handedness" of a chiral SWNT. The obtained crystal structure corresponded to a 1D fragment extracted from the valentinite form of Sb_2O_3, as opposed to the senarmontite form (Figure 3d), which was used to simulate the structure (Figure 3e). In this instance, we have only

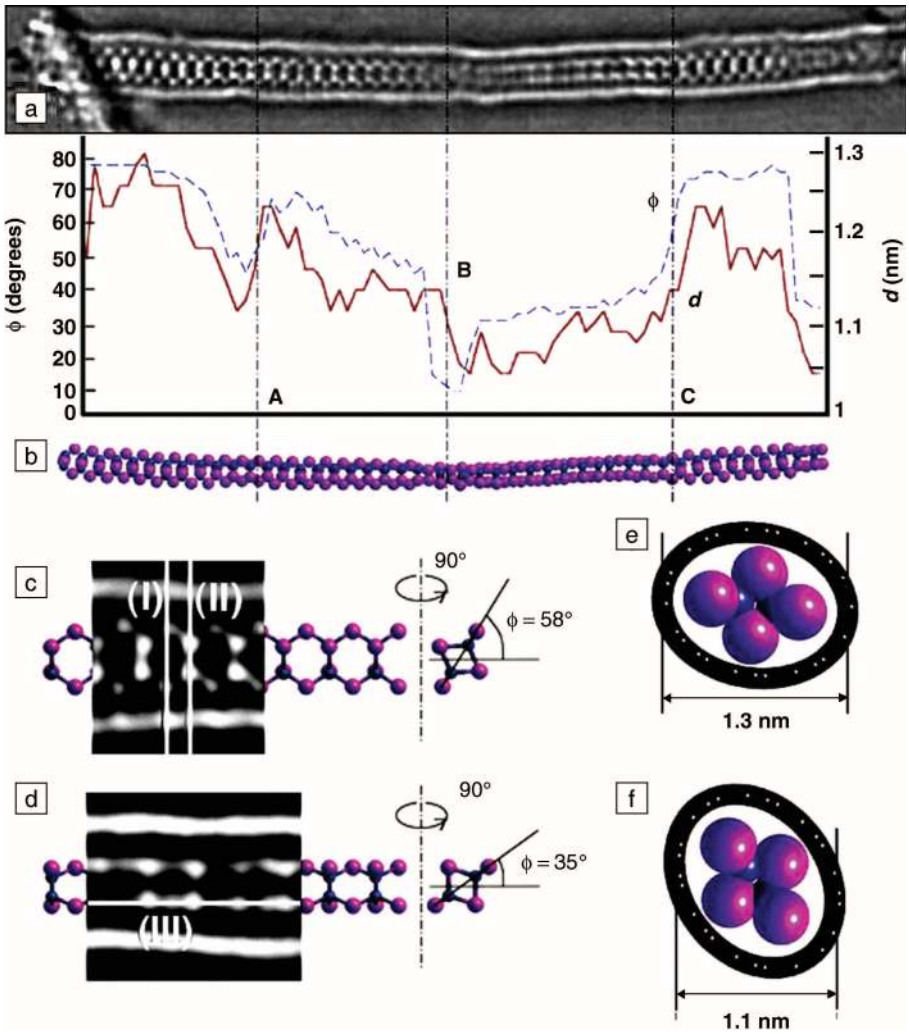

Figure 4. (a) Super-resolved high-resolution transmission electron micrograph produced from a composite between a one-dimensional (1D) CoI_2 crystal and a distorting single-walled carbon nanotube (SWNT). The plot shows the variation of SWNT diameter d *together with the angle of rotation (ϕ) of the Co_2I_4 motif within the encapsulated 1D crystal. (b) Derived structure model. (c), (d) Details from left and right middle sections of (a), showing the microstructure of the 1D crystal in two of the different projections effected by the crystal rotation. Line profiles through* ***I****,* ***II,*** *and* ***III*** *were used to confirm the whole crystal structure of the twisting fragment. (e), (f) End-on views of Co_2I_4 units in two different orientations, showing how the diamond configuration of the I atoms causes an oval distortion in the encapsulating nanotube. (From Reference 40.)*

been able to resolve the strongly scattering Sb^{3+} columns, while the O^{2-} columns were lost in the image noise, probably due to staggering. The column thicknesses of the Sb^{3+} columns (see Figure 2c), extracted from the restored phase, were measured to be 3-3-2-3-3.

In both of these examples, we can extract some clues concerning the 3D nature of the SWNT encapsulates from the presumed geometry of the nanotube, the phase shifts observed for individual atom columns, and the measured tilt angle of the nanotube. This is relatively easy for comparatively symmetrical 1D crystals (such as KI), but quite difficult for more asymmetrical cases. In the special case of a twisted 1D crystal, however, we can extract the entire 1D crystal structure, provided that the same microstructure is maintained along the imaged length of the nanocomposite.[40] In Figure 4a, we see the reconstructed phase of two sections of a distorting SWNT continuously filled with CoI_2. Detailed analysis of the structure of these fragments shows that they differ from the bulk form of the iodide, which can be described as stacked 2D layers of edge-sharing CoI_6 octahedra in which the anions form an hcp lattice.

Figure 4c is a detail obtained from the reconstructed phase and shows that the chain consists of two alternating pairs of atom columns, separated by 0.54 nm and 0.26 nm distances measured perpendicular to the SWNT axis, respectively. Inspection of the whole fragment along the indicated regions **A**, **B**, and **C** in Figure 4a suggests that this same microstructure is maintained along the length of the SWNT. Single-pixel-width line profiles at **I**, **II**, and **III** (Figures 4c and 4d) were therefore used to produce an accurate 3D picture of the whole structure (which is consistent with a Co_2I_4 repeating unit), with the central columns along **II** corresponding to I-Co and Co-I columns, and with the peripheral atom columns measured along **I** corresponding to single-I columns only. It can be seen that this fragment rotates in a fairly smooth fashion along the SWNT capillary (although there is an abrupt rotation at **B**, Figure 4a), and the angle of rotation of the Co_2I_4 subunit (ϕ) was estimated from the 2D projection (see Figures 4c and 4d). The longitudinal line profile at **III** therefore indicates the microstructure of the 1D CoI_2 nanocrystal in a different orientation. A remarkable feature of this nanocomposite is that the asymmetric Co_2I_4 subunits (Figures 4e and 4f) cause a corresponding distortion in the encapsulating nanotube and, furthermore, that this distortion follows the Co_2I_4 subunit rotation along the length of the SWNT. The correlation between the angle of rotation (ϕ) and SWNT diameter *d* can be seen in the graph in Figure 4a.

It is also possible to image SWNT nanocomposites using spatially resolved electron energy-loss spectroscopy (EELS), a technique referred to as spectroscopic imaging. Suenaga et al. have demonstrated that individual gadolinium atoms within endofullerenes are incorporated within SWNTs.[41] These atoms can be imaged by conventional HRTEM due to their high atomic number, but they can also produce a sufficient signal to give a significant EEL spectrum. By scanning a 0.5 nm electron probe over a SWNT filled with $Gd@C_{82}$ endofullerenes, it was possible to produce separate carbon and gadolinium element maps for the sample and to locate the single atoms within the endofullerenes. Such experiments open the way for performing single-atom spectroscopy in an electron microscope.

STM and STS of Fullerenes inside SWNTs

For the development of practical applications, we need to be able to make direct physical measurements on SWNT encapsulates, and this has been spectacularly demonstrated within the last couple of years.[42,43] Scanning tunneling spectroscopy (STS) measurements performed within a scanning tunneling microscope (STM), combined with the atomic resolution provided by the STM, have permitted measurement of the bandgap modulation of both encapsulated fullerenes and endofullerenes. In Figure 5, we reproduce the data obtained from C_{60} peapods. In the first instance, the corrugation of the STM image contrast produced by incorporated fullerene molecules under positive-bias versus negative-bias imaging conditions is clearly visible (Figures 5b–5d). Second, spatially resolved current/voltage (*dI/dV*) spectra obtained in the STS mode (Figures 5e–5f) clearly show how the incorporated molecules modify the bandgap of the encapsulating SWNT. Using an STM tip, it was possible to move the fullerene molecules out of the way and re-record the *dI/dV* spectra, revealing an unmodulated SWNT (dotted curve, Figure 5f).[42] Using similar imaging conditions, it has been possible to measure the bandgap modulation properties of endohedral metallofullerenes (i.e., $Gd@C_{82}$) within SWNTs.[43] In this case, an even larger

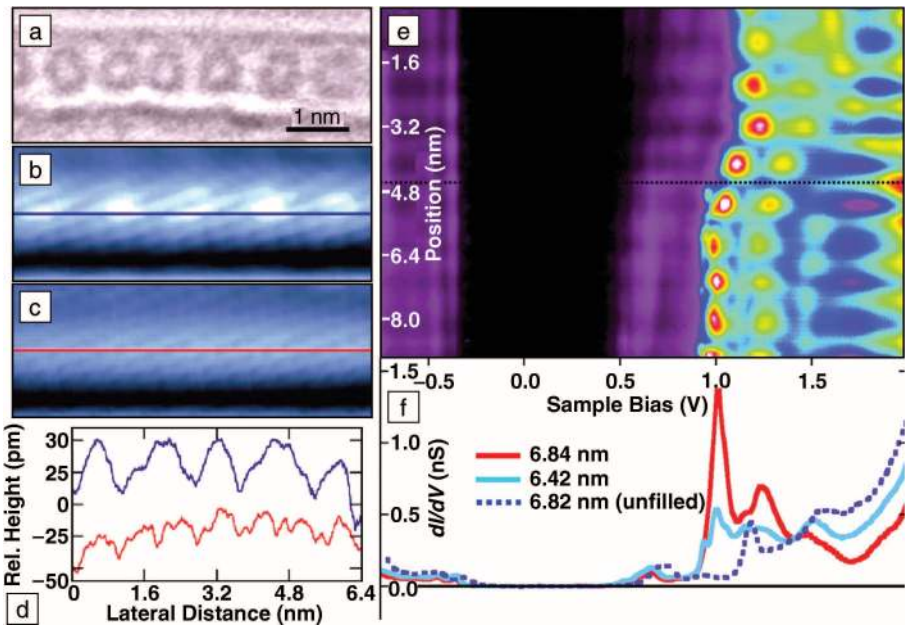

*Figure 5. (a) High-resolution transmission electron micrograph of a single-walled carbon nanotube peapod containing a close-packed one-dimensional chain of C_{60} molecules. (b) Scanning tunneling micrograph of a peapod with a comparable structure to (a), imaged at 4 K and under positive sample bias. (c) is the same view as (b), but was obtained under negative sample bias. (d) Plot showing differences in corrugation (blue line = positive bias; red line = negative bias) under the two imaging conditions. The modulation of the sample bias due to the incorporated C_{60} molecules is clearly visible. (e) Intensity plot of current/voltage (*dI/dV*) measured as a function of voltage bias (*x* axis) and position along the top of the peapod (*y* axis). (f) Representative *dI/dV* spectra as a function of bias obtained from two locations (red curve = over C_{60}; solid blue curve = over vacancy; dashed line = after molecules removed). (From Reference 42.)*

bandgap modulation was observed that was associated with charge transfer between the molecules and the SWNT.

Summary and Future

In this article, we have outlined a variety of bulk and local-scale characterization methodologies for the comprehensive characterization of composites of encapsulated molecules and 1D crystals formed within SWNTs. These are objects that are formed on an atomic scale and as such represent the capability limits of fabrication and characterization technologies. In this regard, they may be considered ideal nanoscale test objects for investigating fundamental structure–property relationships in theoretical physics and also for achieving directly observable chemistry on the molecular scale. As the drive toward the miniaturization of electronic materials and devices progresses, the methodologies described here may be useful in exerting control over electronic states in nanostructures and turning them into something useful.

Acknowledgments

In Oxford and in Pennsylvania, we are deeply indebted to a large number of coworkers and collaborators without whom this work would have been impossible. In Oxford, we would like to thank E. Philp, D.A. Morgan, R. Carter, P.M.F.J. Costa, G. Brown, S.R. Bailey, S. Friedrichs, R.R. Meyer, K.S. Coleman, E. Flahaut (now at CNRS, Toulouse), R.E. Dunin-Borowski (now at Cambridge), and also Owen Saxton from Cambridge University. In Pennsylvania, we would like to thank B.W. Smith, A.T. Johnson, and E.J. Mele. We are also grateful to M. Monthioux (CNRS, Toulouse), D.J. Hornbaker, S.J. Kahng (now at Soongsil University, Korea), S. Misra, and A. Yazdani from the University of Illinois. We are grateful for financial support from the EPSRC, the Leverhulme Foundation, the Royal Society, the Department of Energy, the National Science Foundation, and the Office of Naval Research.

References

1. J. Sloan, A.I. Kirkland, J.L. Hutchison, and M.L.H. Green, *J. Chem. Soc., Chem. Commun.* (2002) p. 1319.
2. Z. Yao, H.W.Ch. Postma, L. Balents, and C. Dekker, *Nature* **402** (1999) p. 273.
3. R.D. Antonov and A.T. Johnson, *Phys. Rev. Lett*. **83** (1999) p. 3274.
4. C. Zhou, J. Kong, E. Yenilmez, and H. Dai, *Science* **290** (2000) p. 1552.
5. S.J. Tans, A.R.M. Verschueren, and C. Dekker, *Nature* **393** (1998) p. 49.
6. H.W.Ch. Postma, T. Teepen, Z. Yao, M. Grifoni, and C. Dekker, *Science* **293** (2001) p. 76.
7. T. Rueckes, K. Kim, E. Joselevich, G.Y. Tseng, C.-L. Cheung, and C.M. Lieber, *Science* **289** (2000) p. 94.
8. A. Bachtold, P. Hadley, T. Nakanishi, and C. Dekker, *Science* **294** (2001) p. 1317.
9. J. Sloan, J. Hammer, M. Zweifka-Sibley, and M.L.H. Green, *J. Chem. Soc., Chem. Commun.* (1998) p. 347.
10. J. Sloan, D.M. Wright, H.G. Woo, S. Bailey, G. Brown, A.P.E. York, K.S. Coleman, J.L. Hutchison, and M.L.H. Green, *J. Chem. Soc., Chem. Commun.* (1999) p. 699.
11. T.W. Ebbesen, *J. Phys. Chem. Solids* **57** (1996) p. 951.
12. G. Brown, S.R. Bailey, M. Novotny, R. Carter, E. Flahaut, K.S. Coleman, J.L. Hutchison, M.L.H. Green, and J. Sloan, *Appl. Phys. A* **76** (2003) p. 1.
13. J. Mittal, M. Monthioux, H. Allouche, and O. Stephan, *Chem. Phys. Lett.* **339** (2001) p. 311.
14. S. Friedrichs, J. Sloan, M.L.H. Green, J.L. Hutchison, R.R. Meyer, and A.I. Kirkland, *Phys. Rev. B* **64** 045406 (2001).
15. X. Fan, E.C. Dickey, P.C. Eklund, K.A. Williams, L. Grigorian, R. Buczko, S.T. Pantelides, and S.J. Pennycook, *Phys. Rev. Lett.* **84** (2000) p. 4621.
16. B.C. Satishkumar, A. Taubert, and D.E. Luzzi, *J. Nanosci. Nanotech.* **3** (2003) p. 159.
17. G. Brown, S.R. Bailey, J. Sloan, C. Xu, S. Friedrichs, E. Flahaut, K.S. Coleman, M.L.H. Green, J.L. Hutchison, and R.E. Dunin-Borkowski, *J. Chem. Soc., Chem. Commun.* (2001) p. 845.
18. B.W. Smith, M. Monthioux, and D.E. Luzzi, *Nature* **396** (1998) p. 323.
19. B.W. Smith, R.M. Russo, S.B. Chikkannanavar, and D.E. Luzzi, *J. Appl. Phys.* **91** (2002) p. 9333.
20. H. Kuzmany, R. Pfeiffer, C. Kramberger, T. Pichler, X. Liu, M. Knupfer, J. Fink, H. Kataura, Y. Achiba, B.W. Smith, and D.E. Luzzi, *Appl. Phys. A* **76** (2003) p. 449.
21. K. Hirahara, K. Suenaga, S. Bandow, H. Kato, T. Okazaki, H. Shinohara, and S. Iijima, *Phys. Rev. Lett.* **85** (2000) p. 5384.
22. F. Stercel, N.M. Nemes, J.E. Fischer, and D.E. Luzzi, *Making Functional Materials with Nanotubes,* edited by P. Bernier, P. Ajayan, Y. Iwasa, and P. Nikolaev (Mater. Res. Soc. Symp. Proc. **706**, Warrendale, PA, 2002) p. 245.
23. D.A. Morgan, J. Sloan, and M.L.H. Green, *J. Chem. Soc., Chem. Commun.* (2002) p. 2442.
24. T. Takenobu, T. Takano, M. Shiraishi, Y. Murakami, M. Ata, H. Kataura, Y. Achiba, and Y. Iwasa, *Nat. Mater.* **2** (2003) p. 683.
25. S. Rols, R. Almairac, L. Henrard, E. Anglaret, and J.L. Sauvajol, *Eur. Phys. J. B* **10** (1999) p. 263.
26. Y. Maniwa, H. Kataura, M. Abe, A. Fujiwara, R. Fujiwara, H. Kira, H. Tou, S. Suzuki, Y. Achiba, E. Nishibori, M. Takata, M. Sakata, and H. Seumatsu, *J. Phys. Soc. Jpn.* **72** (2003) p. 45.
27. H. Kataura, Y. Maniwa, M. Abe, A. Fujiwara, T. Kodama, K. Kikuchi, H. Imahori, Y. Misaki, S. Suzuki, and Y. Achiba, *Appl. Phys. A* **74** (2002) p. 349.
28. M. Kociak, K. Hirahara, K. Suenaga, and S. Iijima, *Eur. Phys. J. B* **32** (2003) p. 457.
29. S. Iijima, *Nature* **345** (1991) p. 56.
30. M. Gao, J.M. Zuo, R.D. Twesten, I. Petrov, L.A. Nagahara, and R. Zhang, *Appl. Phys. Lett.* **82** (2003) p. 2703.
31. J.M. Zuo, I. Vartanyants, M. Gao, R. Zhang, and L.A. Nagahara, *Science* **300** (2003) p.1419.
32. Ch. Kramberger, R. Pfeiffer, H. Kuzmany, V. Zólyomi, and J. Kürti, *Phys. Rev. B* **68** 235404-1 (2003).
33. K. Hirahara, S. Bandow, K. Suenaga, H. Kato, T. Okazaki, H. Shinohara, and S. Iijima, *Phys. Rev. B* **64** 115420-1 (2001).
34. J. Sloan, M.C. Novotny, S.R. Bailey, G. Brown, C. Xu, V.C. Williams, S. Friedrichs, E. Flahaut, R.L. Callendar, A.P.E. York, K.S. Coleman, M.L.H. Green, R.E. Dunin-Borkowski, and J.L. Hutchison, *Chem. Phys. Lett.* **329** (2000) p. 61.
35. A.I. Kirkland, W.O. Saxton, and G. Chand, *J. Electron Microsc.* **46** (1997) p. 11.
36. W. Coene, G. Janssen, M. Op de Beeck, and D. van Dyck, *Phys. Rev. Lett.* **69** (1992) p. 3743.
37. R.R. Meyer, A.I. Kirkland, and W.O. Saxton, *Ultramicroscopy* **92** (2002) p. 89.
38. Y. Shao-Horn, L. Croguennec, C. Delmas, C.E. Nelson, and M.A. O'Keefe, *Nat. Mater.* **2** (2003) p. 464.
39. R.R. Meyer, J. Sloan, R.E. Dunin-Borkowski, A.I. Kirkland, M.C. Novotny, S.R. Bailey, J.L. Hutchison, and M.L.H. Green, *Science* **289** (2000) p. 1324.
40. E. Philp, J. Sloan, A.I. Kirkland, R.R. Meyer, S. Friedrichs, J.L. Hutchison, and M.L.H. Green, *Nat. Mater.* **2** (2003) p. 788.
41. K. Suenaga, M. Tencé, C. Mory, C. Colliex, H. Kato, T. Okazaki, H. Shinohara, K. Hirahara, S. Bandow, and S. Iijima, *Science* **290** (2000) p. 2280.
42. D.J. Hornbaker, S.-J. Kahng, S. Misra, B.W. Smith, A.T. Johnson, E.J. Mele, D.E. Luzzi, and A. Yazdani, *Science* **290** (2002) p. 828.
43. J. Lee, H. Kim, S.-J. Kahng, G. Kim, Y.-W. Son, J. Ihm, H. Kato, Z.W. Wang, T. Okazaki, H. Shinohara, and Y. Kuk, *Nature* **415** (2002) p. 1005. □